Computational Analysis of the Utilisation of the Shape Memory Effect and Balloon Expansion in Fully Polymeric Stent Deployment

ANNA C. BOBEL and PETER E. MCHUGH

Biomechanics Research Centre (BMEC), Biomedical Engineering, College of Engineering and Informatics, NUI Galway, Galway, Ireland

Associate Editors James E. Moore, Jr. and Ajit P. Yoganathan oversaw the review of this article.

Abstract—The desire to overcome the limitations of cardiovascular metal stents is driven by the global clinical need to improve patient outcomes. The opportunity for fully polymeric stents made from materials like Poly-L-lactide Acid (PLLA) is significant. Unfortunately, this potential has not been fully realised due to pressing concerns regarding the radial strength and recoil associated with material stiffness and recoverability. In an effort to achieve effective and reliable performance, it is conceivable that a certain degree of shape memory effect (SME) could be beneficial in order to improve on high recoil associated with fully polymeric stents. In this paper, a computational model is presented to explore this possibility, using a stent geometry based on that of a commercially available polymeric stent (Abbott Absorb). The model predicts improvements in the recoil behaviour if the stent is subjected to temperature changes (introducing the shape memory effect to the material) prior to implantation compared to balloon inflation alone. The analysis indicates that combination of self-expansion and balloon inflation is capable of reducing stent recoil to a desirable level (5%). Additionally, the analysis suggests that the recoil is not strongly related to expansion rate variation. However, the stent expansion rate is critically linked to the maximum stresses in the material, with significantly higher stresses found if the stent was deployed with a higher rate, leading to a significantly higher material failure risk. It is concluded that the model provides new insights that can guide the development of fully polymeric stents towards optimised clinical performance with the potential to improve patient outcomes.

Keywords—PLLA, Cardiovascular stent, Shape memory effect, Finite element analysis.

INTRODUCTION

The clinical problems (i.e. restenosis and thrombosis) associated with traditional stents are well documented.[27,29] Numerous reports strongly indicate that these post deployment issues are in part caused by the material mismatch and permanent nature of metal stents.[11,26,32] The desire to improve patient outcomes has encouraged the exploration of fully polymeric stents because of their ability to disappear after deployment.[28] In particular, Poly-L-lactide Acid (PLLA) as a stenting material has been evaluated with a small number of commercial offerings on the market.[8,21,24]

The potential paradigm shift to fully polymeric stents is promising; however, the pace of clinical adoption for those limited number of products commercially available has proved slow. As described by Bobel *et al.*,[4,6] there is a lack of long term data in relation to the reliable mechanical performance of fully polymeric stents. More specifically, there are major concerns in regards to their reliability from a stiffness standpoint and stent recoil that may influence load carry capacity and associated risk.[4,19,20]

A study reported by Bobel *et al.* presents analysis of the radial compressibility of a PLLA stent without the specific consideration of shape memory effect (SME). Interestingly, it was demonstrated that the fully polymeric PLLA stent could only provide satisfactory radial support if the elastic modulus is improved significantly, relative to "standard" values, by polymer composition variations or alternative manufacturing techniques.[4]

To further support this line of thought, a large amount of polymeric biodegradable stent patents have been granted by industry leaders, in particular Abbott Vascular. A patent entitled "Manufacturing process

Address correspondence to Anna C. Bobel, Biomechanics Research Centre (BMEC), Biomedical Engineering, College of Engineering and Informatics, NUI Galway, Galway, Ireland. Electronic mail: a.bobel1@nuigalway.ie

for polymeric stents"[17] by Abbott, published in 2015, details (claims) the manufacturing process of a fully polymeric stent comprised of the following steps:

(i) Forming a polymeric tube with a diameter less than the target diameter.
(ii) Radially deforming the tube to the target diameter at a temperature above glass transition temperature Tg, and finally cutting the stent pattern into the deformed tube.[17]

The crimping method for these stents is described in complimentary patents by Abbott Vascular.[16,22] More specifically, under temperatures of between Tg and 15 degrees below Tg, the scaffold is crimped on to a balloon. It is stated that semi-crystalline polymers, such as PLLA, can improve on their retention force by controlling the temperature in relation to Tg.[16] If a PLLA stent is crimped at room temperature, the free movement of polymer chains cannot occur. Therefore, it can be challenging to crimp a stent with a large diameter to a designated smaller diameter. On the one hand, the stent can be crimped with a higher force, which can likely lead to fracture/damage within the material. Alternatively, a slower crimping rate can reduce the fracture/damage risk, but cannot ensure no damage. However, developing the crimping process to include a temperature increase can help to deform the stent to a reduced diameter without causing negative effects to the mechanical properties of the polymer. Summarising the above, controlled temperature increase can positively influence the crimping process. Another crucial parameter for fully polymeric stents development is the deformation rate, which can have a critical impact on the material fracture during deformation.

In another patented issued by Abbott, it is stated that without further processing, polymers such as PLLA do not have the adequate strength and fracture toughness for reliable and fit for purpose performance.[5,12,13] In practice, the concept of the SME in fully polymeric stents was effectively introduced with the very first CE approved biodegradable polymer stent (PLLA, and deployed using a combination of balloon and self-expansion) the "Igaki-Tamai" stent.[25] The SME appears at 65 °C, the typical glass transition temperature for PLLA. However, as this temperature ranges well above the body temperature, it raised many concerns regarding tissue trauma and damage. Since the self-expanding SME approach presents an opportunity to improve on some of the main issues related to fully polymeric biodegradable stents, primarily in relation to stiffness and recoil, this phenomenon needs to be further investigated. In particular, in order to create a functional SME, that can be safely used

in vivo, the self-expanding component needs to be introduced at body temperature.

The material of interest, PLLA, has a glass transition temperature Tg of 65 °C. Therefore the pressing question is raised if shape memory can be introduced at a lower temperature, close to body temperature. A study by Lan *et al.*[18] investigated this, focused on the example of shape memory polymer composites and their recovery at Tg, Tg + 10 °C, Tg – 10 °C and Tg – 20 °C. The results of Lan *et al.*[18] showed that the strain recovery is superior at temperatures closest to the glass transition temperature. However, there is still visible shape memory recovery at temperatures above/below Tg.

To investigate the implications of the findings of Lan *et al.*[18] for the stent application, i.e. assuming the existence of shape memory recovery at temperatures below Tg, a computational study is proposed herein with the aim of implementing a representation of the SME at body temperature. Specifically, a computational modelling framework is designed to implement a representation of the SME at body temperature in polymeric stents. Using this, a computational study is undertaken that compares the SME with the more commonly used balloon deployment method in relation to stent deployment behaviour and recoil performance. Specifically, deployment techniques based on balloon expansion, self-expansion and a combination of these two methods, are analysed to assess possible improvements in stent recoil and material fracture risk.

MATERIALS AND METHODS

Material Model

The Parallel Rheological Framework (PRF), depicted in Fig. 1 was utilised in this study, as available in the Abaqus 6.14 commercial software Package (DS SIMULIA, USA), as the material model. Features of this model (Fig. 1) include the combination of elastic, viscous and plastic elements, temperature dependency and significantly, the model can be used with Abaqus/Explicit, which enables flexible implementation for the solution of highly non-linear, large deformation problems such as stent expansion.

The basic structural assumption of the PRF-network used in this study, is two network arms layout (network arm #0 and #1, as per Fig. 1b), with an added plastic element to the equilibrium network (network # 0) as shown in Fig. 1b. Therefore (hyperelastic) elastic, plastic and viscous elements needed to be defined.

The PRF model offers a choice of Hyperelastic and viscous elements. The elastic element representation in
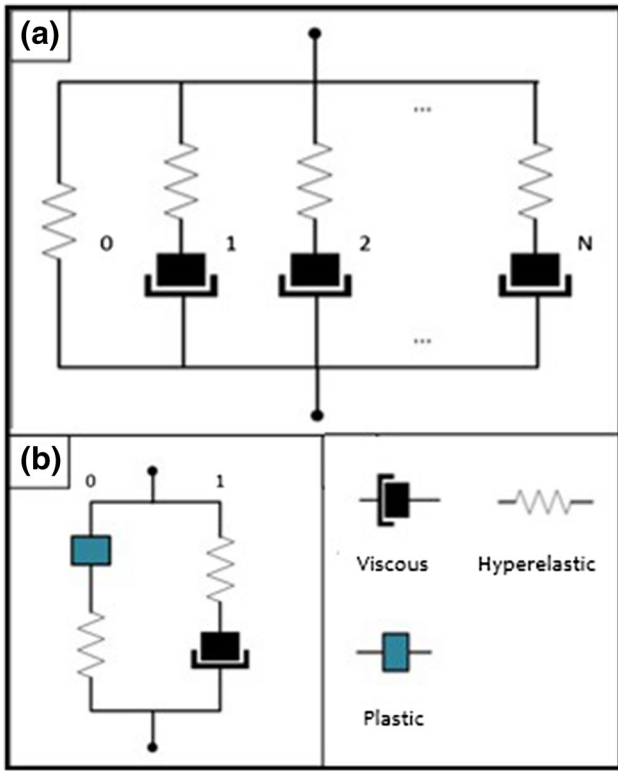
FIGURE 1. (a) PRF network, (b) PRF network including plastic element and one additional network arm.

this study is specified as the Neo-Hookean hyperelastic model, which is able to predict the nonlinear stress–strain behaviour of materials undergoing large deformation. The following strain energy density function for this model is readily implemented in Abaqus:

$$U_{\text{NH}} = C_{10}(\bar{I}_1 - 3) + \frac{1}{D_1}(J^{\text{el}} - 1) \tag{1}$$

where, J^{el} is the elastic volume ratio (Jacobian), is the deviatoric counterpart of the invariant $\bar{I}_1 = J^{-2/3} I_1$, C_{10} and D_1 are shear and bulk material property constants, respectively.

The viscoelastic element is defined by the Bergstrom-Boyce creep strain rate model, which has been reported previously as a reasonable representation for PLLA biodegradable semi-crystalline thermoplastic when used in a parallel network.[10] This viscous model is defined in Abaqus as follows

$$\dot{\bar{\varepsilon}}^{\text{er}} = A(\lambda^{\text{er}} - 1 + E)^C (\tilde{q})^m \tag{2}$$

with

$$\lambda^{\text{er}} = \sqrt{\frac{1}{3} \boldsymbol{I} : \boldsymbol{C}^{\text{er}}} \tag{3}$$

where $\dot{\bar{\varepsilon}}^{\text{er}}$ is the equivalent creep strain rate, $\tilde{q}$ the deviatoric Kirchhoff stress, and A, m, E and C are material parameters.

TABLE 1. Overview of elements used in the PRF model.

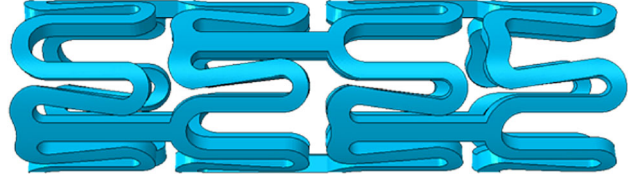| Element type	Material law	Input parameters
Hyperelastic	Neo Hookean	C_{10}, D_1
Viscoelastic	Bergstrom–Boyce	A, m, C, E
Plastic	Isotropic hardening	σ_{yield}, $\varepsilon_{\text{plastic}}$

FIGURE 2. Abbott Absorb stent geometry in Abaqus.

The plastic element is added to the network as shown in Fig. 1b, which is assumed to represent a permanent set in rubber-like materials. This behaviour is captured by isotropic hardening von Mises plasticity with an associated flow rule. In the context of finite elastic strains associated with the underlying rubber-like material, in Abaqus plasticity is modelled based in multiplicative split of the deformation gradient $\boldsymbol{F}$ into elastic $\boldsymbol{F}^{\text{el}}$ and plastic $\boldsymbol{F}^{\text{pl}}$ components

$$\boldsymbol{F} = \boldsymbol{F}^{\text{el}} \cdot \boldsymbol{F}^{\text{pl}} \tag{4}$$

Based on this, the input parameters required are listed in Table 1.

Computational Model and Simulations

The simulation sequence used in this work, described below, was implemented into Abaqus/Explicit. Abaqus/Explicit was used as it affords greater computational robustness in achieving a successful solution, in comparison to Abaqus/Standard, in a case such as this that involves large deformation, highly non-linear material behaviour, temperature variation, and changes in elastic and plastic material properties. For the study reported here, initial work with Abaqus/Standard resulted in numerical problems, due to difficulties in achieving convergence for the implicit solution method.

A realistic stent geometry (as shown in Fig. 2) capturing the Abbott Absorb stent design pattern, was created in Abaqus.[4] The stent strut thickness as well as the stent diameter matched the patterns used by Bobel et al.,[4] with a strut thickness of 156 μm, strut width of 144 μm and a fully expanded diameter of 3.0 mm. The finite element type used, to combine temperature as well as displacement within an explicit simulation process, was an 8-noded thermally coupled brick element, with linear interpolation in each of the 3 direc-

tions in 3D and temperature variation and with reduced integration. The time scaling factor has been set to 1 with a target time increment of 1×10^{-4}. A representation of the shape memory effect was introduced based on a stress free initial expanded stent geometry. The stent was fixed in all directions, other than circumferential, using displacement based boundary conditions. The initial temperature was set to 20 °C to represent room temperature. Two cylindrical shapes (as shown in Fig. 3) were added to the simulation: Cylinder 1 representing a stent crimping tool with a slightly larger initial diameter than the stent; Cylinder 2 representing the balloon the stent is crimped onto, to be used to expand the stent during balloon deployment. Both cylinders were created using a rigid cylinder, a simplification to a real geometry balloon, evaluated and justified previously by Grogan et al.[15] The finite element mesh used for the stent model itself was that used in previous published studies, in particular Bobel et al.[4] and for those studies the mesh suitability for stent deployment simulation was
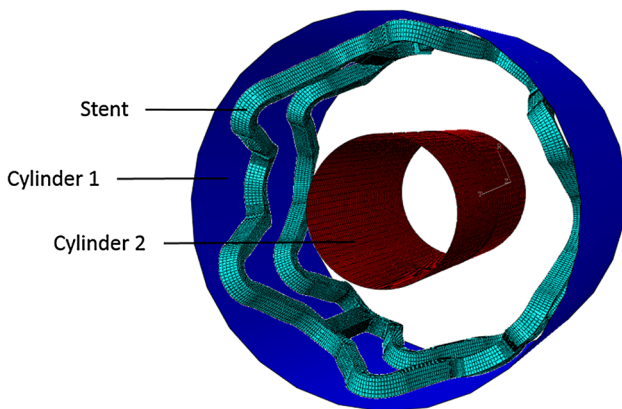
established, including the use of stent mesh densities previously reported.[7,15]

In the first step of the simulation, temperature was applied to increase the initial temperature from 20 to 39 °C (see Fig. 4). The next step, called crimp-cool, employed the crimping using Cylinder 1 of the stent onto the balloon (Cylinder 2); in the very last instant of the crimping process, the stent was cooled down to 15 °C. The reheat-recovery step increased the temperature back to 39 °C, at the same time Cylinder 1 displaced outwards to allow the stent to freely recover. The balloon was expanded when the stent reached the state of maximum free recovery, so that the stent expanded even further to a pre-set diameter. Finally, the balloon was contracted (deflated) during the recoil step to allow the stent to freely recoil. The timeline of this process that represented the inclusion of the shape memory effect, referred to here as the "shape memory cycle", and the corresponding temperature history, is summarised in Fig. 4.

Recoil Assessment

A primary focus of this computational study is the recoil behaviour of the fully polymeric stent. Pure PLLA material properties, especially the elastic modulus, may be too low to withstand the forces experienced during stent deployment. For this reason, a computational study was performed using direct-experimentally calibrated values, vs. enhanced values, as detailed below:

Recoil is defined using the following equation[15]

$$\text{Recoil}(\%) = \frac{D_1 - D_2}{D_1} \times 100 \qquad (5)$$

where D_1 is the external diameter at maximum expansion and D_2 the external diameter following balloon deflation.

FIGURE 3. Computational stent model set-up, consisting of Cylinder 1, Cylinder 2 and stent.
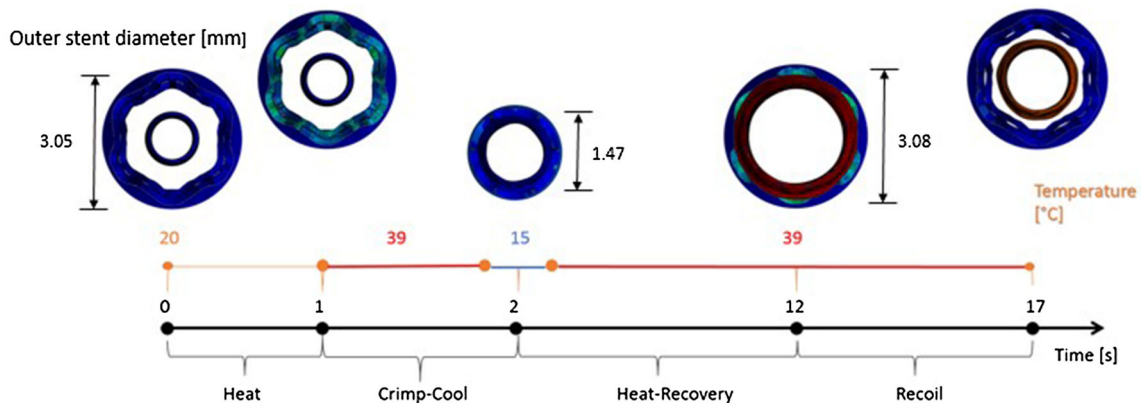

FIGURE 4. Timeline of the shape memory cycle and associated balloon deployment with step times on the black axis and temperatures on the orange axis.

Deployment and Recoil

Three different types of recoil behaviour are compared in this study, related to three different deployment methods:

    I. Self-expansion deployment—the use of the SME for stent deployment through free recovery self-expansion.

    II. Combined deployment—stent deployment as in I, but with additional balloon expansion.

    III. Balloon-expansion deployment—the stent is deployed through balloon expansion only.

Material Fracture Strength

Sufficient material fracture strength is essential for safe stent deployment. Hence the maximum stresses during stent deployment were compared, typically at the point of full expansion. A reference value for PLLA was taken in order to determine the material failure risk. The different deployment methods and expansion rates were compared in terms of the material fracture risk.

Expansion Rate Dependency

The variation of the stent expansion rate was analysed by the adjustment of the time frame of the balloon expansion. The stent expansion rate is defined as the radial displacement of the stent per unit of time. The rates chosen for this study ranged from 2.5 to 30 mm/min and are reflective of the real stent deployment indications [1]. The recoil behaviour and fracture risk were compared as a function of expansion rate. Table 2 highlights the actual deployment duration for different expansion rates, where the expansion rate is shown with the associated deployment duration time, which consists of self-expansion time (free recovery) plus balloon deployment time.

RESULTS

Material Model Calibration and Parameter Fitting

The material model calibration was based on an experimental study previously reported by Bobel et al.[6]

TABLE 2. Deployment times.

Expansion rate (mm/min)	Deployment duration (s) (self-expansion + balloon)
2.5	6 + 18
7.5	6 + 6
10	6 + 4.5
20	6 + 2.25
30	6 + 1.5

The material model was calibrated based on the experimental tensile results for PLLA at room and body temperature as well as different displacement rates. Furthermore, recovery of the material was considered for implementation into the material model.

Initial Model Behaviour

As the material model is complex, in particular for the viscous element, an initial study was undertaken to gain a better understanding of the viscous element behaviour. A Mathematica (Wolfram, USA) routine was developed to illustrate the effects of varying the input parameters in the viscous element, and this initial study was performed before the main model calibration to understand the significance of the viscous material parameters. The numerical analysis was performed based on a 1D case study. A first set of constants was used for this routine (see Table 3), and one constant was varied each time within a range found in literature,[3,9] at (a) constant strain (generating a 2D plot) (b) increasing strain using three different displacement rates (generating a 3D plot). The Bergstrom-Boyce creep strain rate definition, shown in Eqs. (2) and (3) was used for the initial study.

$$\text{Assuming } \lambda^{\text{er}} - 1 = \varepsilon$$

Equation (2) leads to following

$$\dot{\bar{\varepsilon}}^{\text{er}} = A(\varepsilon + E)^C (\tilde{q})^m \tag{6}$$

Solving for the stress, the following equation is obtained and was implemented in Mathematica

$$\tilde{q} = \left[\frac{\dot{\bar{\varepsilon}}^{\text{er}}}{A(\varepsilon + E)^C} \right]^{\frac{1}{m}} \tag{7}$$

Figure 5 shows a stress–strain relationship using the input data in Table 3 and three different displacement rates. The specific ranges have been evaluated by (i) experience using this model, (ii) parameter recommendations found in publications.[3] An overview is given in Table 4, linking the strain rates to the displacement rates, referred to in this study. The maximum strain was selected to be 0.5 (representative of strain ranges experienced locally in the current application), and stress was subsequently calculated as a function of strain. A nearly linear relationship of

TABLE 3. Initial input constants for the Bergstrom–Boyce model.

A (s^{-1})	m	C (MPa^{-1})	E
2.0×10^{-7}	2.0	-1.0	0.3

stroess and strain could be observed with the selected input parameters.

In Fig. 6 the same input data was used, and additionally includes a variation of A in the range $0 \leq A \leq 1$. The Mathematica output Fig. 6a shows the stress vs. A at different displacement rates, and an exponential decrease in stress with an increasing value of A was observed. Plot b in Fig. 6 presents a 3D visualisation of stress and strain vs. A. A significant stress decrease was found with an increasing value of A, where the main dependence was observed within a smaller value range of A ($0 \leq A \leq 0.3$). Approaching the upper limit of A ($0.4 \leq A \leq 1$), only a minor decrease on the stress levels was observed. With regard to the rate dependency, a shift in the positive direction for stress was found with increasing displacement rates.

A similar plot is shown in Fig. 7, once again using the input data from Table 3, but where the parameter E was varied in the following range: $0 \leq E \leq 1$. Summarising, an increase in E was found to cause a nearly linear increase in stress (Fig. 7a). The rate dependency can be described in a similar way to above: a positive curve shift with increasing strain rates. In Fig. 7b the stress–strain relationship is shown as a function of the parameter E, and the main stress increase is visible at relatively low strains up to 0.2.

Figure 8 shows the effects of the variation of the constant C, which is defined between $-1 \leq C \leq 0$. C is recommended to be kept $\sim -1^3$ in order to reproduce

the exact inverse function of $A(\lambda^{er} - 1 + E)$, however, the effects of the variation of C in above range was analysed here. Overall C was found to have relatively little impact on the overall stress output (Fig. 8a); an increase in stress with an increasing value of C was observed to follow a linear trend, but with a very low slope. However, the displacement rate dependency was found to be significant with an increase in stress with increasing displacement rates. Again the stress–strain behaviour, shown in the 3D plot in Fig. 8b, follows a consistent pattern as a function of C.

Lastly, the variation in the constant m was analysed within a range of $0 < m \leq 5$, with all other parameters held constant according to Table 3. Figures 9a and 9b show a major effect on the stress output in a value range up to ~ 3. For values $m > 3$ little to no effect was observed. This constant was also found to strongly influence the rate dependency in the same range (up to ~ 3), but beyond this the material was essentially rate independent.

The above Mathematica viscous element input parameter analysis provides a clear understanding of the importance of each of the material parameters, and their range of influence, for use in the Bergstrom-Boyce model as part of the PRF. The complexity of the highly non-linear PRF model and its individual elements requires a clear understanding of the behaviour of each element in order to fit the experimental data in a practical and sensible way. The information generated above enabled a fit of experimental data to be performed very efficiently in relation to the Bergstrom-Boyce element. More specifically, the parameters with a rather non-linear dependence behaviour (such as A and m), could be defined within a more sensible range. A number of iterative steps, following this initial fitting exercise, was performed in order to sensibly adjust these non-linear dependence values based on the determined range.

Material Model Fitting

The material model fitting was performed based on the experimental data presented in Bobel et al.[6] In this study, thin film samples (thickness of 200 μm) were produced from PLLA (Purasorb PL 65) using the solvent casting technique. The testing specimens had a gauge length of 10 mm and a width of 4 mm. A uniaxial tensile test was performed that focused on material recovery, relaxation and strain-rate dependency. Two fitting exercises were performed: experimental data fitted at room temperature for different displacement rates (Fig. 10), and data fitted for the material recovery at room temperature and body temperature for a constant displacement rate (Fig. 11). The resulting version of the PRF model was able to
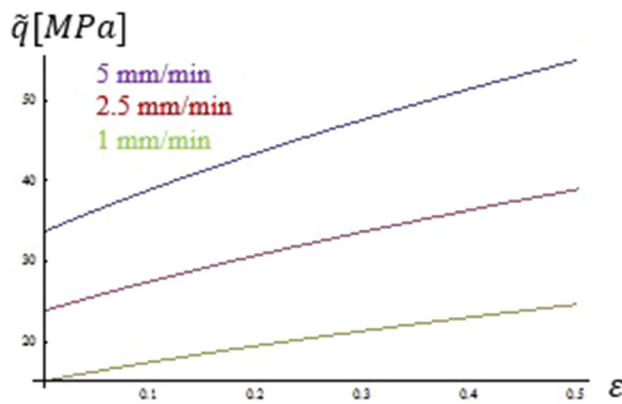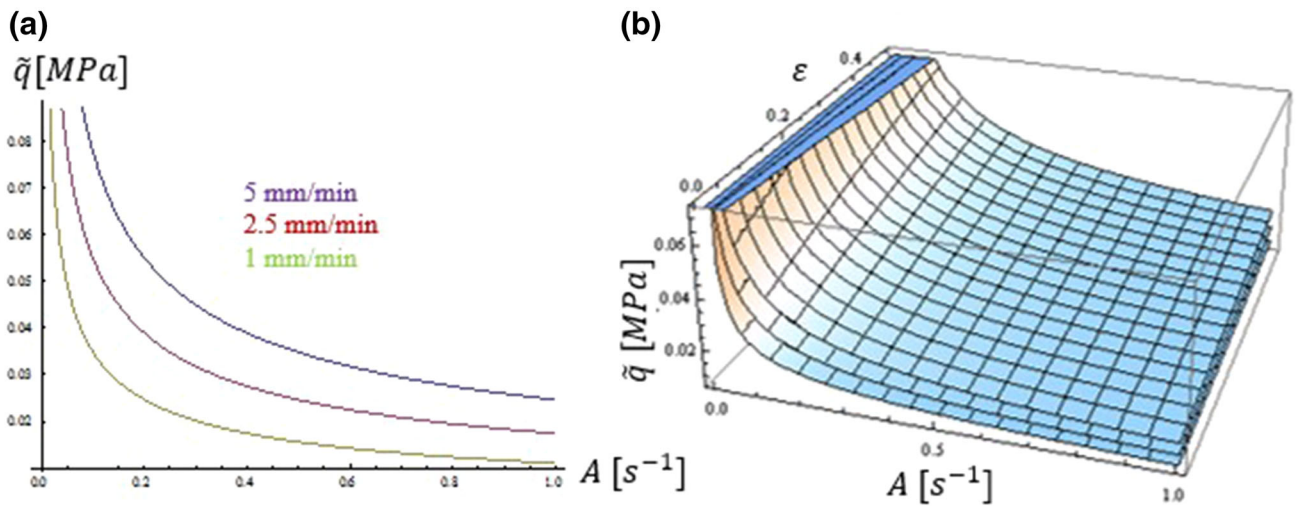
FIGURE 5. Stress-strain curves using input parameters in Table 3, for three different displacement rates.

TABLE 4. Displacement rates and corresponding strain rates for the presented Mathematica study.

Displacement rate (mm/min)	Strain rate (s^{-1})
5 $\cong$	7.58×10^{-4}
2.5 $\cong$	3.79×10^{-4}
1 $\cong$	1.52×10^{-4}

(a)

(b)

FIGURE 6. Variation of A vs. stress (a) and variation of A vs. stress and strain (b) for three different displacement rates.
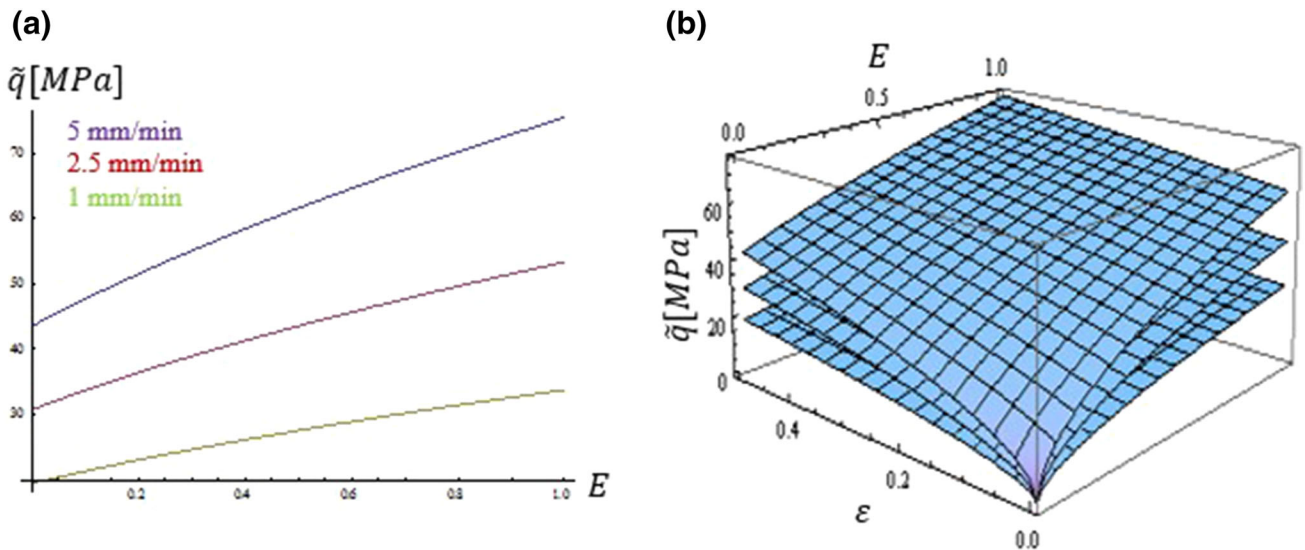
(a)

(b)

FIGURE 7. Variation of 'E' vs. stress (a) and variation of 'E' vs. stress and strain (b) for three different displacement rates.

capture the material behaviour up to 50% deformation, as well as the recovery.

As mentioned, the material properties for PLLA can vary depending on manufacturing technique, material composition and testing set-up. For this reason, a modified material fit at body temperature was implemented, as shown in Fig. 12, where the initial elastic stiffness was increased. The experimental fit at room was left unchanged as the material stiffness is sufficient at that temperature, and in particular the deployment process (as per the three methods previously described is performed at constant body temperature of 39 °C (Heat-Recovery and Recoil Steps in Fig. 4), meaning the material behaviour at body temperature is of pri-

mary importance. The modified material fit is based on material properties found in literature.[14,30,31,33] More specifically, the initial elastic response, which was found to have a major effect in the polymer stent performance pre-degradation,[4] was stiffened by the increase in the initial elastic modulus at body temperature, from the experimentally determined value of 0.272 GPa,[6] to a value of 0.655 GPa. The modified value agrees with alternative experimental data found in literature for PLLA, such as Weir et al.[30] As already presented in a publication by Bobel et al.,[6] the elastic modulus can strongly depend on the material processing method. As already indicated, the initial elastic response defines the material stiffness, and as a result
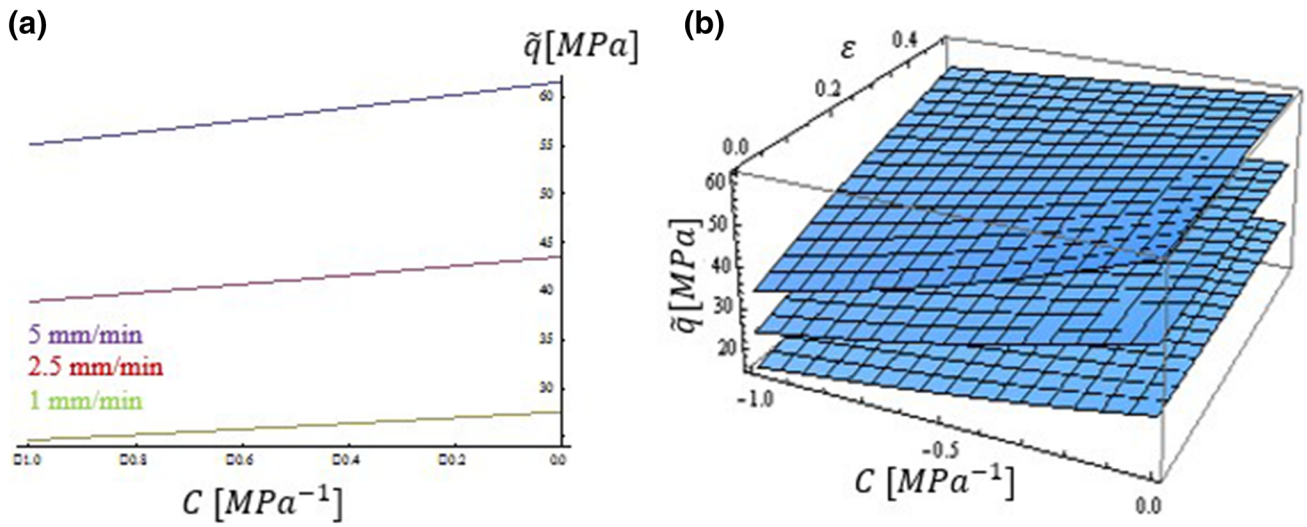
(a)

(b)

FIGURE 8. Variation of C vs. stress (a) and variation of C vs. stress and strain (b) for three different displacement rates.
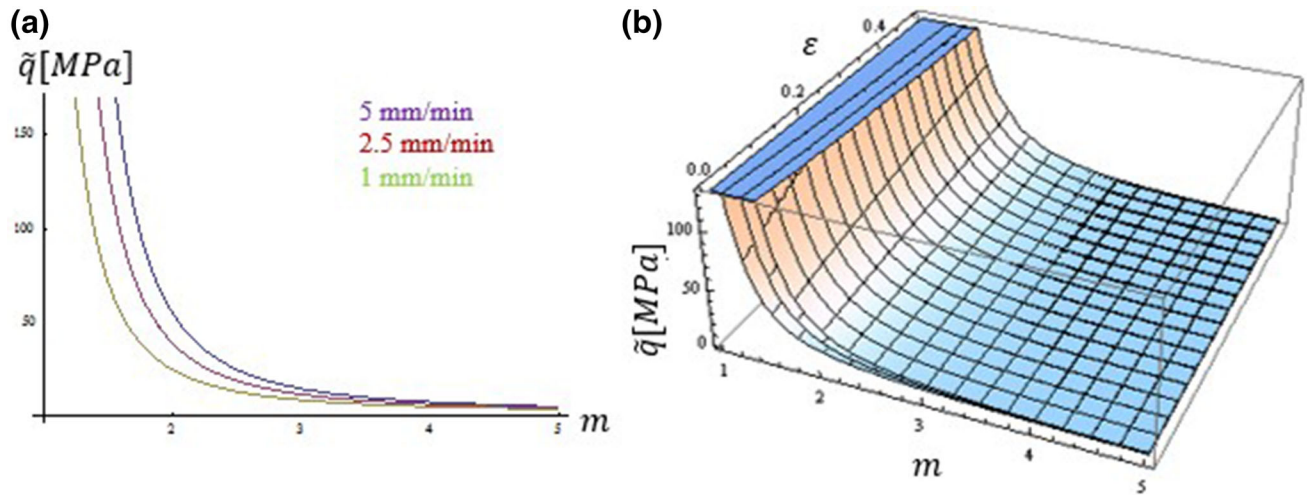
(a)

(b)

FIGURE 9. Variation of 'm' vs. stress (a) and variation of 'm' vs. stress and strain (b) for three different displacement rates.
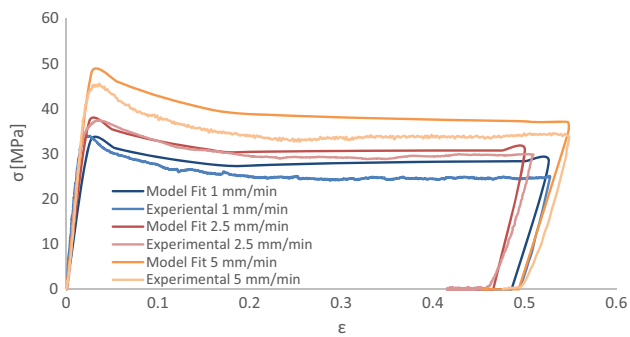

FIGURE 10. Fit to experimental data[6] at room temperature (RT) and different displacement rates.
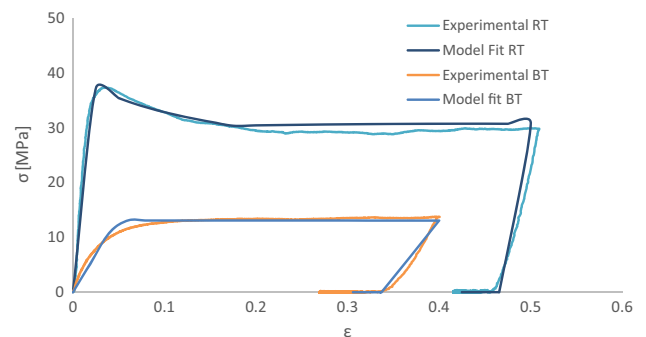

FIGURE 11. Fit to experimental data[6] at constant displacement rates of 2.5 mm/min and different temperatures (room temperature (RT) and body temperature (BT), including material recovery.

the unloading slope and elastic recovery behaviour are improved, with positive implications for stent recoil.

Table 5 Input material parameters with temperature dependency. Below shows the fitted parameters used for the simulations (with reference to Figs. 11 and 12). Parameter set 1 was fitted to the initial experimental data, and set 2 improves the material stiffness based on comparisons to other published experimental data.[14,30,31,33] A parameter variation study was performed to generate the set of material model input parameters. Similar to the study reported by Bobel et al.,[4] the modified parameter set was systematically iterated until a reasonable correlation with experimental data published in literature was found to ensure sufficient stiffness of the polymeric stent.

Deployment Method

The recoil behaviour is an essential characteristic for reliable and safe stent deployment, and in general little or no recoil is desirable. The recoil characteristics strongly depend on the material choice and the related material properties. In this study, the stent alone was examined by focussing on the performance of the polymer material without the inclusion of in vivo conditions such as artery, pulsatile forces or flow.

Figure 13 shows the first result: a comparison of recoil behaviour for the different deployment methods,
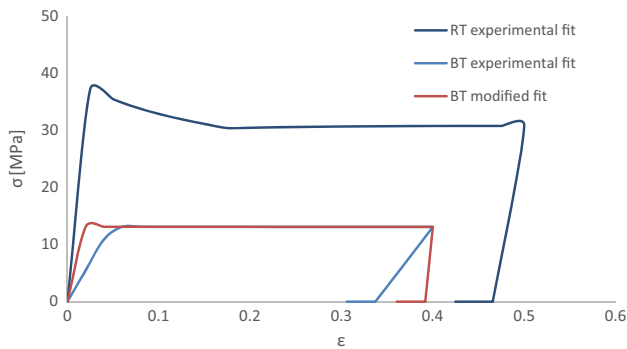
using the modified material parameter set. The difference in recoil for each deployment method is clearly visible: The combined deployment offers the least recoil with 5%, followed by the balloon expansion with 20% and the self-expansion with 34%.

Figure 14 provides a comparative analysis of the expansion rate dependency for all three methods, using the modified material parameter set. It is observed that the recoil is not strongly dependent on the rate of stent deployment, for two of the deployment methods. The trend line for self and combined recoil show negligible expansion rate dependency, whereas the balloon recoil shows increasing recoil with an increase in expansion rate (recoil between 16 and 67%). Figure 15 shows the
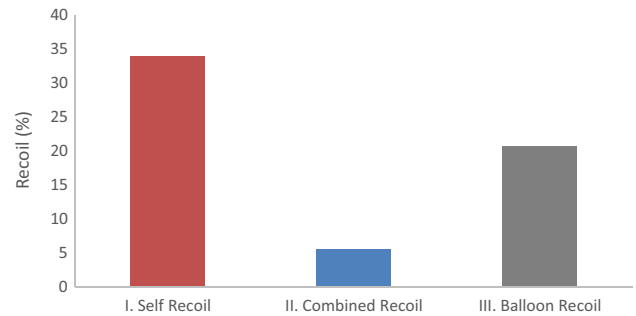
FIGURE 13. Stent Recoil calculated for different deployment methods at constant expansion rate of 7.5 mm/min.

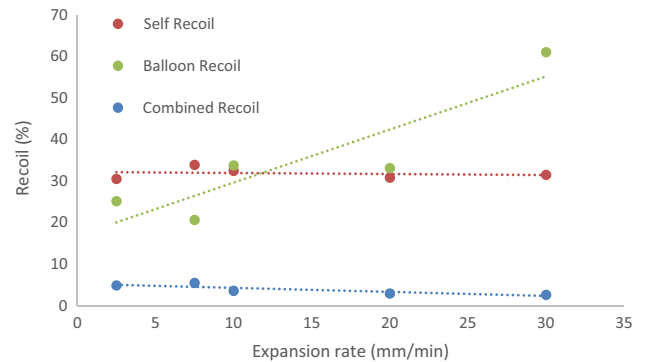FIGURE 12. Modified fit at RT and BT and constant displacement rate of 2.5 mm/min.

FIGURE 14. Stent recoil for different deployment techniques and varying expansion rates.

TABLE 5. Input material parameters with temperature dependency.

	Viscous material constantsBergstrom–Boyce model				Hyperelastic constantsNeo-Hookean model	
	A (s^{-1})	m	C (MPa^{-1})	E	D_1 [MPa^{-1}]	C_{10} (MPa)
1						
RT experimental	4.4×10^{-3}	0.6	-1	0.3	1000	3.8×10^{-5}
BT experimental	4.4×10^{-2}	0.6	-1	0.3	100	3.8×10^{-5}
2						
BT modified fit	4.4×10^{-2}	0.6	-1	0.3	800	3.8×10^{-5}

comparison of % recoil for the experimental vs. modified material parameter fits. A major improvement in recoil is visible for the combined deployment
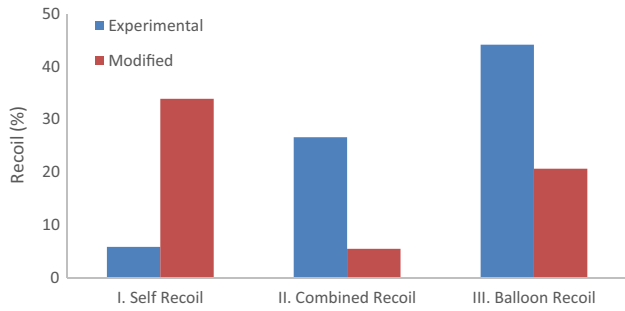

FIGURE 15. Stent recoil for experimentally determined input data vs. modified material data.
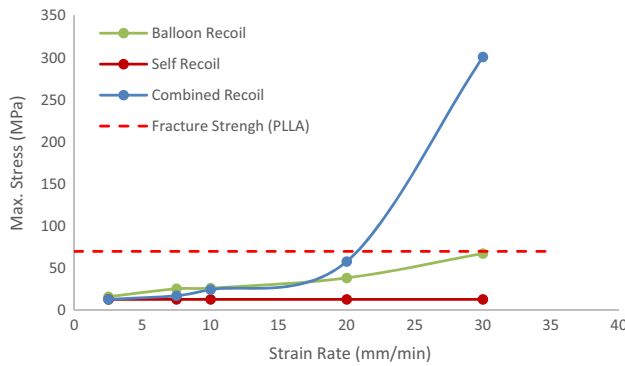

FIGURE 16. Von Mises stress in the stent during deployment to highlight the possibly of material fracture at different expansion rates and due to deployment techniques.

method, and a slightly lower improvement for the balloon deployment. However, the opposite characteristics are observed for the self-expansion; the material property modification significantly increases the % recoil.

Material Fracture Strength

Material fracture during deployment is a well-known performance related issue for fully polymeric stents.[23] The stress (maximum von Mises stress) within the material at maximum stent expansion is shown in Fig. 16 as a function of expansion rate. The red line shows the maximum allowed stress before fracture for PLLA.[2] It can be observed that the stress increases significantly with increasing expansion rate. The balloon expanded stent as well as the combined expanded stent show a similar increase in stress. However, at a displacement rate above 15 mm/min, the combined deployment method induces a significant increase in stress compared to the balloon expansion. All results under the red line can be considered in the safe deployment zone. The results for the self-expanded stent were not added into Fig. 16 as the maximum stress was found to be rate independent. The reason being that the free expansion of the stent, is purely guided by the ability of the material to recover, not driven by an external force. The stress distribution throughout the stent is also shown in Fig. 17 in more detail.
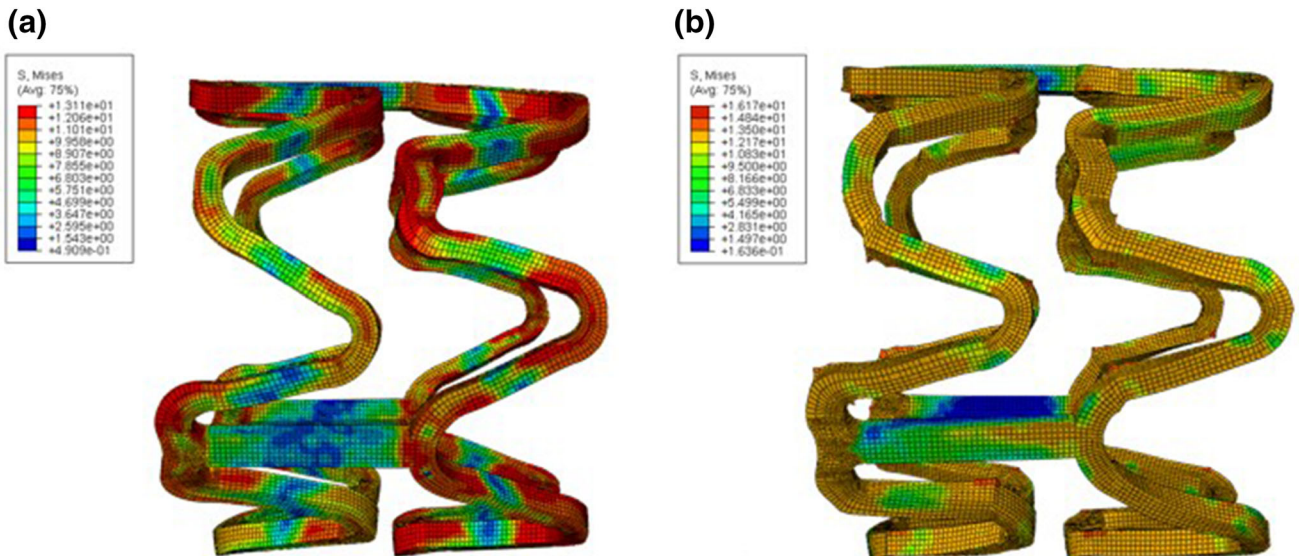

FIGURE 17. Von Mises stress contribution throughout the stent geometry at 2.5 mm/min expansion rate, a max. Von Mises stress for a combined deployment, b max. Von Mises stress for balloon deployment.

DISCUSSION

In this study a computational model was developed to predict the material behaviour of PLLA, as well as to evaluate the effect of SME in fully polymeric stents. Since the radial strength, recoil and material fracture of fully polymeric stents still present concerns among the cardiovascular experts,[23,29] a computational framework can be beneficial to evaluate the deployment process and eliminate related risks.

The experimental data gathered in [[6]] was used to calibrate the PRF network model. To capture different scenarios of stent expansion and temperature variation, the model was calibrated to the experimental data over a range of displacement rates and temperatures. Since the experimental data used to fit the material model relied on pure PLLA, prepared and tested in one specific way,[34] a second set of input parameters was created in order to capture a larger range of material stiffness.

Findings previously reported by Bobel et al.[4] pointed towards the need for an improvement in material stiffness. Stents were characterised and bench tested in terms of their polymeric material properties and suitability for coronary stent application. Developing on this previous study, the computational analysis presented in this paper looked at the deployment method and recoil.

The recoil for three different options of stent deployment was analysed in Fig. 13. This study highlights the effect of temperature and related shape memory characteristics, and in particular those found at close to body temperature. The results indicate that the degree of shape memory found at body temperature has the potential to improve on material recoil. As a consequence of this, the assumption that some degree of SME is included in the functionality of commercially available polymer stents is supported. The recoil found at a constant expansion rate (2.5 mm/min) with combined, balloon and self-deployment, of respectively 5–20–34%, indicates the strong improvement of recoil with a combination of SME and balloon expansion compared to balloon expansion or self-deployment. In conclusion, the combined deployment technique showed an improvement in recoil of 15% compared to balloon expansion, and 29% compared with self-expansion.

It is clear that the choice of deployment technique has a major impact of the stent recoil performance, given that an improvement of 29% was found among the tested deployment options (combined vs. self-deployment). As part of this, the results indicate that pure self-expansion is not satisfactory for polymer stents, and that the most effective aspect of deployment is the combination of self and balloon expansion. Since shape memory at lower temperature happens very slowly[18] the balloon can help to speed up this process so that equilibrium between recoil and outward memory force is accomplished. This method clearly improves the recoil compared to commonly used balloon expansion.

It was also shown that the rate of expansion does not have a major impact on the recoil behaviour of combined and self-expanding stent deployment (see Fig. 14). However, it was noted that the recoil after balloon deployment increased at higher expansion rates. In this case this can be understood since slow deformation enhances the plastic flow and therefore enhances the recoil behaviour, relative to the behaviour at higher rates. Since the recommendation for the deployment of polymer stents[1] advises a slow and steady stent expansion, the expansion rate is clearly of importance for polymer stent deployment. Related to this, the stress level at full expansion, as a function of the expansion rate (see Fig. 16) was analysed. A significant increase in stresses (from 60 to 300 MPa) was observed at expansion rates over 20 mm/min using the combined deployment technique. The recommended fracture strength for PLLA was defined as 70 MPa,[2] meaning only stent expansion rates < 20 mm/min can guarantee a safe deployment using the combination of self and balloon deployment. However, the maximum stresses found for balloon deployment did not reach the material fracture strength for the tested expansion rates. For the combined deployment, the self-expansion component invokes the ability of the stent to self-recover from an initially pre-expanded state, and this pre-deformation can increase the stresses within the material immensely, leading to a material fracture risk. The stress levels in the material are of relevance as it is known that cracks in the polymer can occur during deployment.[16,23]

Figure 15 compares the recoil behaviour for the modified material parameter fit with original experimental parameter fit. With the parameter modification an improvement of recoil by 20% was gained for the combined deployment, and an improvement of 24% for the balloon expansion. However, the self-expansion showed the opposite pattern, with the recoil increasing by 28%. The increase in material stiffness for the modified material properties leads to the enhanced ability of the material to recover even larger strains. Since the self-expansion of a stent is based on the ability of the material to freely recover strains, a stiffer elastic response can cause increase in recoil behaviour.

Overall, as is clear from Fig. 15, the combined deployment technique showed the best relative improvement in recoil with the use of the modified material parameters.

Overall, due to the viscoelastic nature of PLLA, a slow deployment accomplishes a smoother material deformation and greater plastic flow. From an experimental perspective, this was also concluded based on a PLLA deformation study.[6] To summarise, as supported by the computational results generated here, it is highly recommended to expand the stent with a low rate to improve recoil behaviour and to avoid material failure risk.

LIMITATIONS

The computational modelling framework used in this work gives a very useful indication and understanding of the effects of the deployment technique and deployment rate for fully polymeric stents. The parallel rheological framework (PRF) model used was able to include viscoelasticity, as well as plasticity; however, only the elastic and plastic elements could be altered as a function of temperature. To include full variation of all parameters, a more complex user defined subroutine would need to be developed and implemented. Using this, a more comprehensive study of the effects of temperature change on the stent behaviour and mechanical performance could be undertaken.

The simulations presented here have focused on the mechanical performance of the stent itself. An advancement on this approach would be to add the representation of the artery and diseased tissue (plaque) to the model to improve the representation of the *in vivo* mechanical environment experienced by the stent.

Finally, in relation to polymeric materials, the present study has focused on PLLA, however there is significant scope to consider alternative polymers and co-polymers.

CONCLUSION

This study has considered the development and use of a computational model to assess the effects of the deployment procedure on the recoil and material fracture risk for fully polymeric stents. In particular, deployment through self-expansion (using the SME), balloon expansion and a combination of the two were considered. In relation to stent recoil, the results have indicated that the combined deployment method generates the best results, and that material fracture risk is minimised by utilising a slow stent deployment rate.

While polymer stent design is a complex process, it is anticipated that the computational modelling framework presented here and results generated,

should be of significant practical use to stent designers in developing the next generation of stenting technology.

CONFLICT OF INTEREST

Author Anna C. Bobel and Author Peter E. McHugh declare that they have no conflict of interest.

HUMAN AND ANIMAL RIGHTS AND INFORMED CONSENT

No human and animal studies were carried out by the authors for this article.

REFERENCES

[1]Abbott (2015) Absorb GT1 Bioresorbable Scaffold System. http://eifu.abbottvascular.com/en/index.html.
[2]Anonymous (2010) Datasheet 04. In: Physical Properties. www.purac.com.
[3]Bergström, J., and M. Boyce. Constitutive modeling of the time-dependent and cyclic loading of elastomers and application to soft biological tissues. *Mech. Mater*. 33:523–530, 2001.
[4]Bobel, A., S. Petisco, J. R. Sarasua, *et al*. Computational bench testing to evaluate the short-term mechanical performance of a polymeric stent. *Cardiovasc. Eng. Technol*. 6:519–532, 2015.
[5]Bobel, A. C. Computational and Experimental Analysis to Predict the Short-Term Mechanical Performance of Polymeric Vascular Stents. Galway: Biomedical Engineering, National University of Ireland, 2016.
[6]Bobel, A. C., S. Lohfeld, R. N. Shirazi, *et al*. Experimental mechanical testing of Poly (l-Lactide)(PLLA) to facilitate pre-degradation characteristics for application in cardiovascular stenting. *Polym. Test*. 54:150–158, 2016.
[7]Boland, E. L., J. A. Grogan, C. Conway, *et al*. Computer simulation of the mechanical behaviour of implanted biodegradable stents in a remodelling artery. *JOM* 68:1198–1203, 2016.
[8]Chowdhury, A. W. Bioabsorbable stents: Reaching clinical reality. *Cardiovasc. J*. 6:90–91, 2014.
[9]Dalrymple T (2014) Calibration of Polypropylene. In: Dassault Systemes.
[10]Eswaran SK, Kelley JA, Bergstrom JS et al. Material Modeling of Polylactide. SIMULIA Customer Conference, pp. 1–11.

[11]Finn, A. V., G. Nakazawa, M. Joner, et al. Vascular responses to drug eluting stents. Arterioscler. Thrombosis Vasc Biol. 27:1500–1510, 2007.

[12]Gada MB, Kleiner LW, Steichen BE (filed 30 September 2013, and issued 10 April 2014) Method of fabricating a low crystallinity poly (L-lactide) tube. In: US Patent US20140100649 A1.

[13]Glauser T, Gueriguian V, Steichen B et al. (2013) Controlling crystalline morphology of a bioabsorbable stent. In: US Patent US9211682.

[14]Grabow, N., M. Schlun, K. Sternberg, et al. Mechanical properties of laser cut poly (L-lactide) micro-specimens: implications for stent design, manufacture, and sterilization. J. Biomech. Eng. 127:25, 2005.

[15]Grogan, J., S. Leen, and P. Mchugh. Comparing coronary stent material performance on a common geometric platform through simulated bench testing. J. Mech. Behav. Biomed. Mater. 12:129–138, 2012.

[16]Jow KF, Yang AS, Wang Y et al. (2012) Methods for crimping a polymeric stent onto a delivery balloon. In: Google Patents.

[17]Kleine K, Gale DC, Huang B et al. (2015) Manufacturing process for polymeric stents. In:Google Patents.

[18]Lan, X., Y. Liu, H. Lv, et al. Fiber reinforced shape-memory polymer composite and its application in a deployable hinge. Smart Mater. Struc. 18:024002, 2009.

[19]Migliavacca, F., L. Petrini, M. Colombo, et al. Mechanical behavior of coronary stents investigated through the finite element method. J. Biomech. 35:803–811, 2002.

[20]Mortier, P., M. De Beule, P. Segers, et al. Virtual bench testing of new generation coronary stents. EuroIntervention 7:369–376, 2011.

[21]Staehr P (2012) Absorb bioresorbable vascular scaffold system. In: Vascular A (ed) 17th Asian Harmonization Working Party Annual Conference. Taipei.

[22]Stankus J, Serna B (2014) Methods for uniform crimping and deployment of a polymer scaffold. In: US Patent US9161852.

[23]Stankus JS, Zhao H, Trollsas M et al. (filed 23 July 2012, and issued 3 March 2015) Shape memory bioresorbable polymer peripheral scaffolds. In: US Patent US8968387 B2.

[24]Tamai, H., K. Igaki, E. Kyo, et al. Initial and 6-month results of biodegradable poly-l-lactic acid coronary stents in humans. Circulation 102:399–404, 2000.

[25]Tamai, H., K. Igaki, T. Tsuji, et al. A biodegradable poly-l-lactic acid coronary stent in the porcine coronary artery. J. Interv. Cardiol. 12:443–450, 1999.

[26]Van Der Hoeven, B. L., N. M. M. Pires, H. M. Warda, et al. Drug-eluting stents: results, promises and problems. Int. J. Cardiol. 99:9–17, 2005.

[27]Venkatraman, S., and F. Boey. Release profiles in drug-eluting stents: Issues and uncertainties. J. Controll. Release 120:149–160, 2007.

[28]Waksman, R. The disappearing stent: when plastic replaces metal. Circulation 2012. 10.1161/CIRCULATIONAHA.

[29]Waksman, R. Promise and challenges of bioabsorbable stents. Catheter. Cardiovasc. Interv. 70:407–414, 2007.

[30]Weir, N., F. Buchanan, J. Orr, et al. Processing, annealing and sterilisation of poly-L-lactide. Biomaterials 25:3939–3949, 2004.

[31]Welch, T. R., R. C. Eberhart, S. V. Reddy, et al. Novel bioresorbable stent design and fabrication: Congenital heart disease applications. Cardiovasc. Eng. Technol. 4:171–182, 2013.

[32]Welt, F. G. P., and C. Rogers. Inflammation and restenosis in the stent era. Arterioscler. Thromb. Vasc. Biol. 22:1769–1776, 2002.

[33]Wong, Y., Z. Stachurski, and S. Venkatraman. Modeling shape memory effect in uncrosslinked amorphous biodegradable polymer. Polymer 52:874–880, 2011.

[34]Zienkiewicz, O. C., R. L. Taylor, O. C. Zienkiewicz, et al. The finite element method. London: McGraw-Hill, 1977.